Analysis of a conductive heat flow profile in the Ecuador Fracture Zone

Kannikha Parameswari Kolandaivelu [a], Robert N. Harris [b], Robert P. Lowell [a,*],
Ahmed Alhamad [c,d], Emma P.M. Gregory [c], Richard W. Hobbs [c]

[a] *Department of Geosciences, Virginia Polytechnic Institute and State University, Blacksburg, VA 24061, United States*
[b] *College of Earth, Ocean, and Atmospheric Sciences, Oregon State University, Corvallis, OR 97331, United States*
[c] *Department of Earth Sciences, Durham University, Durham DH1, United Kingdom*
[d] *Saudi Aramco, PO Box: 19673, Al-Midra Building, Dhahran 31311, Saudi Arabia*

ARTICLE INFO

ABSTRACT

We report 18 new conductive heat flow measurements collected from a sediment pond located in the inactive part of the Ecuador Fracture Zone in the Panama Basin. The data were collected along an east–west transect coincident with a multi-channel seismic reflection profile that extends from ODP Hole 504B to west of the sediment pond. Conductive models indicate that heat flow should decrease from ≈ 400 mW m^{-2} on the 1.5 Ma western plate to ≈ 200 mW m^{-2} on the 6 Ma eastern plate; however the observed heat flow increases nearly linearly toward the east from approximately 140 mW m^{-2} to 190 mW m^{-2}. The mean value of 160 mW m^{-2} represents an average heat flow deficit of $\approx 50\%$, which we attribute to lateral advective heat transfer between exposed outcrops on the western and eastern margins of the sediment pond. We apply the well-mixed aquifer model to explain this eastwardly flow, and estimate a volumetric flow rate per unit length in the north–south direction of $\approx 400 \pm 250$ m^2 yr^{-1} through the basement aquifer. Using a Darcy flow model with the mean flow rate, we estimate permeabilities of $\sim 10^{-11}$ and 10^{-12} m^2 for aquifer thicknesses of 100 and 1000 m, respectively. The estimated permeabilities are similar to other estimates in young oceanic upper crust and suggest that vigorous convection within the basement significantly modifies the thermal regime of fracture zones. Additional heat flow data are needed to determine the prevalence and importance of advective heat transfer in fracture zones on a global scale.

1. Introduction

Thermal and mechanical processes affect the tectonic evolution of active oceanic transforms and their fracture zone extensions (e.g., Sandwell, 1984; Pockalny et al., 1996). In addition, these processes influence earthquake mechanics and rheology (e.g., Behn et al., 2007; Roland et al., 2010); and, when combined with fluid circulation, they control the alteration of oceanic crust and serpentinization of the upper mantle (e.g., Dziak et al., 2000) in these regions. In the inactive fracture zone region beyond the active transform, half-space cooling models provide some constraints on the thermal regime of the adjacent plates and the differences in plate age across the fracture zone provide first-order controls on topography (e.g. Menard and Atwater, 1969). The thermal and mechanical behavior of fracture zones is complicated, however, by lateral thermal conduction from the younger to the older plate (e.g.,

Louden and Forsyth, 1976) and by the development of an elastic layer that result in gravitational and topographical features not readily accounted for by simple models (e.g., Sandwell and Schubert, 1982; Sandwell, 1984; Pockalny et al., 1996).

Within and near transform faults and fracture zones heat flow data are sparse; and detailed knowledge of the thermal, mechanical, and possible hydrological regimes is limited. To our knowledge the only other heat flow data from within a fracture zone come from 23 measurements within the thickly sediment Vema transform and fracture zone (Langseth and Hobart, 1976). After correcting for the effects of sedimentation, they find heat flow to be uniform and higher than expected. Other data come from the Ascension fracture zone but are mostly along the flanks of ridge segments (Vacquier and Von Herzen, 1964; Langseth et al., 1966; Von Herzen and Simmons, 1972).

Early thermal models of fracture zones assumed conductive heat transfer. Louden and Forsyth (1976) constructed two-dimensional time dependent models of thermal conduction across an idealized fracture zone and used the resulting temperature structure to calculate free-air gravity anomalies. Behn et al. (2007)

* Corresponding author.
E-mail address: rlowell@vt.edu (R.P. Lowell).
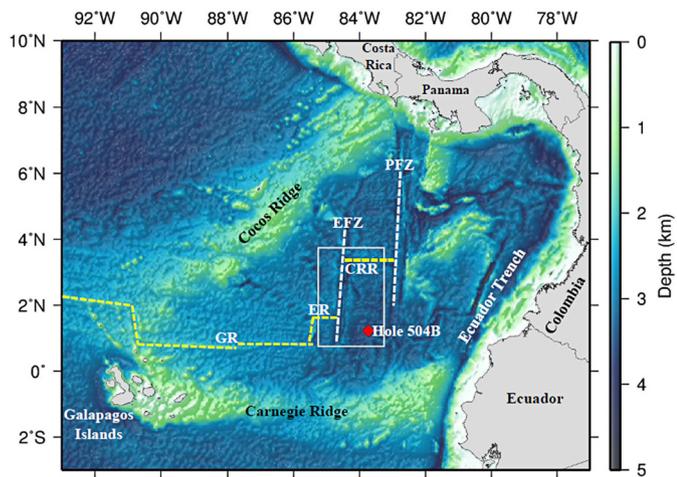
Fig. 1. Map of the Panama Basin. The basin is bounded by the Cocos Ridge to the N and W, the Carnegie Ridge to the S, and the Ecuador Trench and Americas to the E. The dashed yellow lines show the spreading axis (CRR = Costa Rica Rift; ER = Ecuador Ridge; GR = Galapagos Spreading Center). The transforms bounding the CRR, EFZ = Ecuador Fracture Zone; PFZ = Panama Fracture Zone, are labeled and shown in white dashed lines. Red diamond shows the location of the ODP Hole 504B. The white box encloses the area where geophysical measurements were made during cruises JC112, JC113 and Sonne 0238. (For interpretation of the colors in this figure, the reader is referred to the web version of this article.)

constructed three-dimensional models of the thermal structure beneath transforms. These models used a rheology that incorporated brittle weakening of the lithosphere, resulting in elevated temperatures along the transform, and produced better agreement with observed seismicity. Roland et al. (2010) expanded these models to include shear heating and hydrothermal circulation and inferred that hydrothermal cooling has significant effect on the thermal structure of transform faults.

The thermal models of Behn et al. (2007) and Roland et al. (2010) focused on the large scale thermal regime at transform-ridge intersections. The thermal model of Louden and Forsyth (1976), which is more applicable to fracture zones, has not been tested by heat flow data. Relative to heat flow data obtained as a function of age along the flanks of mid-ocean ridges, there has been little attention paid to the details of heat flow and the thermal regime locally around transforms and their fracture zone extensions. Hence, there is essentially no information on heat flow patterns, fluid flow rates, extent of circulation, and subsurface fluid temperatures on a local scale in fracture zone settings.

In this paper, we report 18 conductive heat flow measurements collected across a sediment pond in the Ecuador Fracture Zone south of the Ecuador Rift during the cruises JC113 and JC114 of the OSCAR experiment in the Panama Basin. The data were collected along an east–west transect at a latitude of ∼1°14.0280′N coincident with a multichannel seismic line. We analyze the data using the well-mixed aquifer model.

2. Geologic setting

The Ecuador Fracture Zone (EFZ) consists of the active ridge-transform-ridge offset, that joins the Costa Rica Rift (CRR) in the center of the Panama Basin, the Ecuador Rift (ER) to the southwest of the CRR, and the inactive fracture zones extending to the north of the CRR and south of ER (Fig. 1). Swath bathymetry (Fig. 2) collected during the cruises shows the active and inactive parts of the fracture zone; the region of the heat flow survey, which is located in the inactive part of the EFZ, is depicted by the blue rectangular box. The bathymetry indicates that the EFZ is approximately 20 km wide and is characterized by two linear highs extending for several kilometers along strike. The two
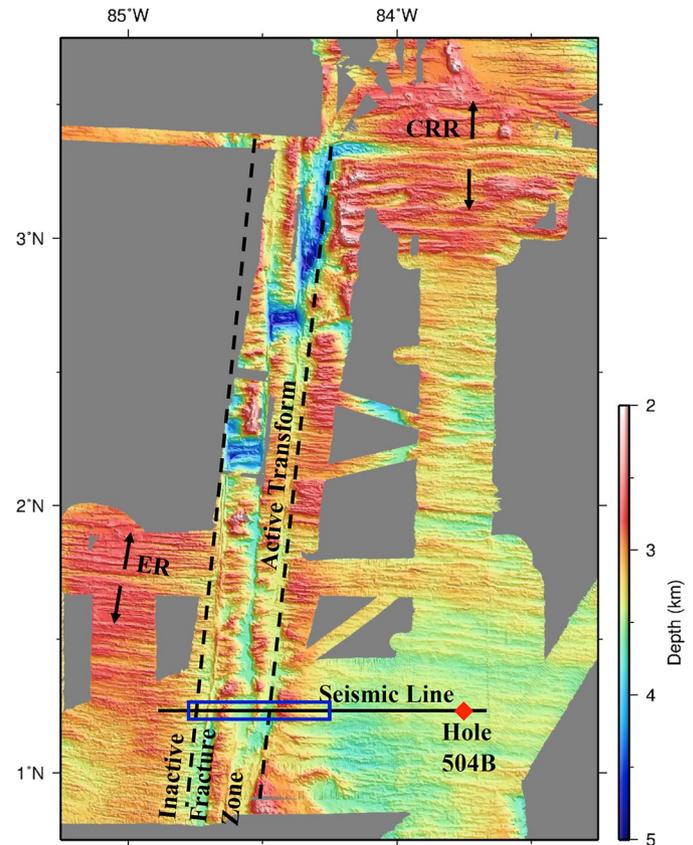

Fig. 2. Bathymetry data showing the EFZ (region bound by black dashed lines). CRR = Costa Rica Rift; ER = Ecuador Ridge. The seismic profile, reproduced in Fig. 3, extends to Hole 504B in the east. The blue box highlights the sediment pond and location of heat flow measurements. The heat flow measurements are collocated with the seismic reflection line. (For interpretation of the colors in this figure, the reader is referred to the web version of this article.)

linear highs form ridges that may have resulted from diaperic uplift of serpentinized-peridotite caused by the intrusion of seawater into the upper mantle via the faults (Kastens et al., 1986; Dziak et al., 2000). In such fracture zones, complex processes shape the hydrogeologic and thermal regime. The sediment pond, where the heat flow measurements were conducted, extends for about 9.3 km in the east–west direction with its center at ∼1°14.0280′N, 84°35.6460′W. The crustal ages to the east and west of the sediment pond are ≈6 and ≈1.5 Ma, respectively, based on spreading rate estimates for the Costa Rica Ridge (Hey et al., 1977; Tuckwell et al., 1996) and distance from ridge axis. Co-locating the heat flow data with seismic reflection data allows us to analyze the heat flow data in the context of sediment thickness and underlying basement structure.

3. Results

3.1. Seismic reflection measurements

A high-resolution seismic profile imaging the sediment structure and top of oceanic crust was acquired using a high-frequency (20–200 Hz) GI airgun source recorded on a 4500 m long hydrophone array with 360 groups spaced at 12.5 m. After merging with the field geometry, the seismic data were high-pass filtered to suppress low-frequency surface wave and ship-tow noise. Figs. 3 and 4a were migrated to give a well-resolved image of the internal structure of the sediments and the sediment-basement interface. The sediment thickness generally increases from west to east across the sediment pond with a mean thickness of approximately
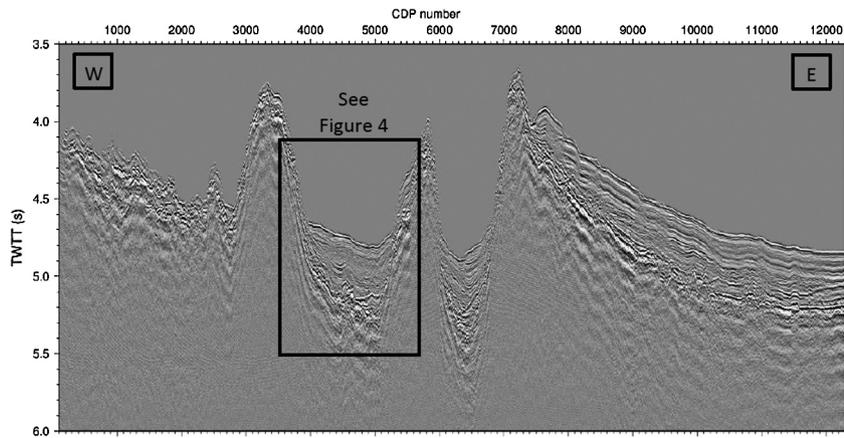
Fig. 3. The post-stack migrated seismic image over the EFZ from west (W) to east (E) along a section of the seismic profile line shown in Fig. 2. The box shows the sediment pond where the heat flow measurements were made. The age of the crust on the west side is 1.5 Ma with predicted basal heat flow $q_b \approx 400$ mW m^{-2} and the age on the east is 6 Ma with $q_b \approx 200$ mW m^{-2}.
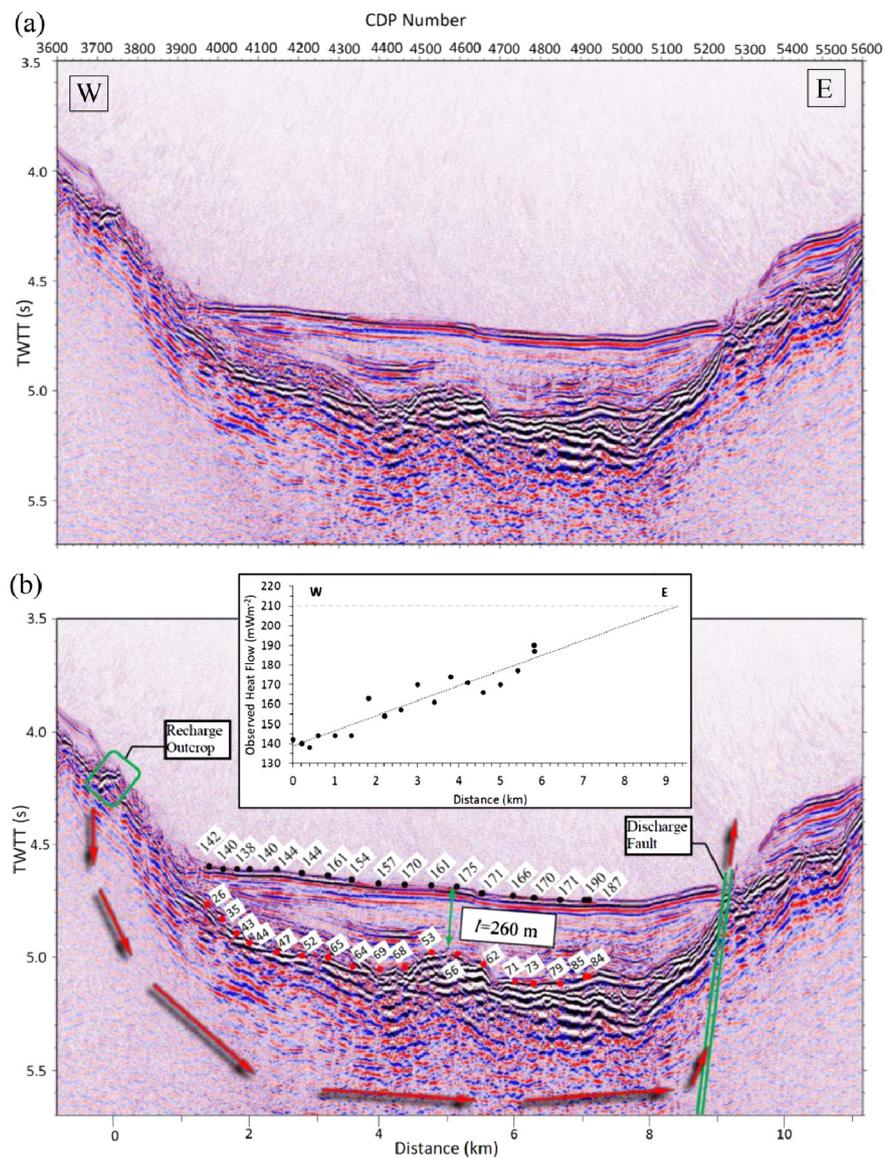
Fig. 4. (a) The pre-stack time migrated seismic image over the sediment pond. The vertical axis is two-way travel time (TWTT). (b) Heat flow data and schematic model of fluid flow. The red arrows indicate the direction of fluid flow. The black circles show the location and value of heat flow measurements in mW m^{-2} (Table 1). Red circles are temperatures at sediment-basement interface in °C (Table 1). The inset displays heat flow as a function of distance and shows the general increase in the observed heat flow from W to E. The black dotted line is the linear trend line determined from Monte Carlo analysis shown in Fig. 6 and red dashed line is the extrapolation of heat flow to 9300 m (discharge fault). l is average sediment thickness. (For interpretation of the colors in this figure, the reader is referred to the web version of this article.)

Table 1
Conductive heat flow data from a sediment pond in the Ecuador Fracture Zone.

Datum	Latitude (°N)	Longitude (°W)	Distance from recharge outcrop[*] (m)	Thermal gradient (°C km^{-1})	Temperature at sediment-basement interface (°C)	Thermal conductivity (W m^{-1} K^{-1})	Heat flow (mW m^{-2})
PB01-01	1.2334	−84.6175	1411 ± 12	193	26	0.7	142 ± 0.5
PB01-02	1.2334	−84.6156	1622 ± 12	193	35	0.7	140 ± 0.2
PB01-03	1.2335	−84.6139	1811 ± 17	196	43	0.7	138 ± 0.4
PB01-04	1.2336	−84.6121	2011 ± 23	191	44	0.8	144 ± 0.4
PB01-05	1.2336	−84.6084	2422 ± 17	188	47	0.8	144 ± 0.4
PB01-06	1.2338	−84.6048	2822 ± 12	196	52	0.7	144 ± 0.4
PB01-07	1.2338	−84.6011	3233 ± 12	231	65	0.7	163 ± 2.4
PB01-08	1.2338	−84.5976	3621 ± 100	214	64	0.7	154 ± 0.6
PB01-09	1.2338	−84.5941	4010 ± 12	217	69	0.7	157 ± 0.3
PB01-10	1.2338	−84.5905	4410 ± 12	224	68	0.8	170 ± 0.5
PB01-11	1.2338	−84.5868	4821 ± 12	226	53	0.7	161 ± 0.6
PB01-12	1.2338	−84.5833	5210 ± 17	253	56	0.7	174 ± 0.3
PB01-13	1.2340	−84.5796	5622 ± 23	247	62	0.7	171 ± 0.4
PB01-14	1.2340	−84.5763	5988 ± 23	235	71	0.7	166 ± 0.7
PB01-15	1.2341	−84.5725	6411 ± 17	242	73	0.7	170 ± 0.6
PB01-16	1.2341	−84.5687	6833 ± 23	244	79	0.7	177 ± 0.4
PB01-17	1.2342	−84.5652	7222 ± 23	274	85	0.7	190 ± 0.5
PB01-18	1.2342	−84.5651	7233 ± 12	211	84	0.9	187 ± 0.4
							Mean heat flow = 160 ± 0.5

[*] Recharge outcrop is considered to be at 0 m.

260 m (Fig. 4a). This image also shows distinct episodes of sediment flux into the basin which may relate to the geological history of the basin as it progressed from the active to passive transform fault system.

3.2. Heat flow data

The conductive heat flow measurements were collected along a 6 km profile in the sediment pond using a multi-penetration heat flow probe (MPHF) consisting of a 3.5 m thermistor string containing 11 thermistors. The violin bow configuration allows repeated measurements during a single transit through the water making it an efficient tool. An ultra-short baseline (USBL) sensor is attached 50 m above the probe to yield precise navigation. Each measurement consisted of both a 7 min measurement period allowing the calculation of sediment equilibrium temperatures and a second 7 min period following a calibrated heat pulse, generated with a heating wire along the thermistor string, so that thermal conductivity could be estimated.

Heat flow was calculated based on the processing algorithm of Villinger and Davis (1987) that allows iterative determination of both the local thermal gradient and values of sediment thermal conductivity (e.g., Stein and Fisher, 2001). Thermal gradients, thermal conductivities and heat flow determinations are displayed in Table 1. Uncertainties are small and based on a Monte Carlo analysis as described in Stein and Fisher (2001). Observed values of heat flow, q_{obs}, increase from approximately 140 to 190 mW m^{-2} toward the east, with a mean value of 160 mW m^{-2} (Fig. 4b). Using the measured thermal conductivity of the sediments and assuming a linear thermal gradient, the temperatures at the sediment-basement interface are calculated from the heat flow observations. These data are also plotted in Fig. 4b.

4. Analysis

For crustal ages less than about 70 Ma, basal heat flow can be predicted using a half space cooling model (Stein and Stein, 1994),

$$q_b = 510 t^{-1/2}, \tag{1}$$

where the age t is in Ma and q_b is the basal heat flow expressed in mW m^{-2}. Table 2 lists the symbols used along with their units and values as appropriate. This model predicts basal heat flow for 1.5 and 6 Ma crust to be ≈400 and ≈200 mW m^{-2}, respectively. One could apply the conductive model of Louden and Forsyth (1976) to obtain an estimate of the effect of lateral conductive transfer across the fracture zone, but because of the complex tectonics within the transform and fracture zone, we calculate the expected heat flow and its uncertainty based on the mean value determined for the young and old plates from equation (1). This calculation gives a mean basal heat flow of ≈300 ± 100 mW m^{-2}. In contrast, the data yield a mean heat flow through sediment pond of 160 mW m^{-2} (Table 1). These values correspond to a mean fractional heat flow deficit $(1 - q_{obs}/q_b)$ of ≈0.5. Moreover, the trend of heat flow values (Fig. 4) is opposite to that expected from lateral conductive heat transfer from the younger to the older plate (Louden and Forsyth, 1976).

The heat flow deficit and trend of observed values could result from rapid sedimentation and/or from lateral advective heat loss due to fluid flow. Rapid sedimentation tends to lower the observed heat flow (e.g., Louden and Forsyth, 1976; Hutchison, 1985; Hutnak and Fisher, 2007). Sediment is usually assumed to be deposited at bottom water temperature and rapid sedimentation can transiently depress heat flow until the sediment warms to equilibrium values (Hutchison, 1985). The potential effect of sedimentation on heat flow can be assessed using scale analysis. If the sediment load in the pond were emplaced instantaneously, the time scale τ for conduction through the sediment pile is,

$$\tau \sim \frac{l^2}{a}, \tag{2}$$

where l is the sediment thickness, and a is the thermal diffusivity of the sediment–water composite medium given by,

$$a = \frac{K_s}{\rho c_p}. \tag{3}$$

Here K_s, thermal conductivity of the sediments, has a nearly constant value of 0.7 W m^{-1} K^{-1} (based on measurements in

Table 2
Parameters and values.

| Symbol	Definition	Value	Units
a	Thermal diffusivity of sediment–water composite medium	2×10^{-7}	$m^2\,s^{-1}$
a^*	Effective thermal diffusivity	2×10^{-7}	$m^2\,s^{-1}$
a_b^*	Effective thermal diffusivity of basement rocks	5×10^{-7}	$m^2\,s^{-1}$
c_f	Specific heat of water	4200	$J\,kg^{-1}\,K^{-1}$
c_s	Specific heat of sediments	1000	$J\,kg^{-1}\,K^{-1}$
g	Acceleration due to gravity	9.81	$m\,s^{-2}$
h_a	Aquifer thickness	100–1000	m
H	Total advective heat loss		$mW\,m^{-1}$
k	Permeability of crustal aquifer		m^2
K_b	Thermal conductivity of the basement rocks	2.0	$W\,m^{-1}\,K^{-1}$
K_s	Thermal conductivity of the sediments	0.7	$W\,m^{-1}\,K^{-1}$
l	Mean sediment thickness	260	m
L	Horizontal fluid flow path length	9300	m
q_{adv}	Mean advective heat flow	140	$mW\,m^{-2}$
q_b	Basal heat flux	$\approx$ 200–400	$mW\,m^{-2}$
q_d	Heat flow at the discharge		$mW\,m^{-2}$
q_{obs}	Mean observed heat flow	160	$mW\,m^{-2}$
Ra, Ra_c	Rayleigh number, and critical value		
t	Age of oceanic crust		Ma
T_d	Temperature at discharge		°C
u	Darcian velocity of fluid		$m\,yr^{-1}$
α	Thermal expansion coefficient of seawater	10^{-4}	$°C^{-1}$
η	Dynamic viscosity of fluid		$kg\,m^{-1}s^{-1}$
ϕ	Porosity of sediments	0.5	
ν	Kinematic viscosity of the fluid	10^{-6}	$m^2\,s^{-1}$
ρ_f	Density of water	1000	$kg\,m^{-3}$
ρ_s	Density of sediments	2300	$kg\,m^{-3}$
τ	Time scale for heat conduction through sediment pile		yrs

Table 1); and ρc_p is the heat capacity of sediment–water composite medium. That is

$$\rho c_p = \rho_s c_s (1 - \phi) + \rho_f c_f \phi, \qquad (4)$$

where ρ_s and ρ_f are the densities of sediment and water respectively, c_s and c_f are the specific heat of sediment and water respectively, and ϕ is the porosity. Using the values as shown in Table 2 in equations (3) and (4), gives $a \approx 2 \times 10^{-7}$ $m^2\,s^{-1}$. Using this value in equation (2), with a mean sediment thickness of 260 m (Fig. 4), yields $\tau \sim 10,000$ yrs. Because the seismic data suggests several episodes of sediment emplacement (Fig. 4), heat flow through the sediment pile should have equilibrated with the basement rock. Hence, sedimentation likely has a negligible effect on the observed heat flow.

The low mean heat flow could also reflect advective loss due to hydrothermal circulation, which could redistribute basal heat flux by lateral fluid flow in the basement rocks. This process is commonly observed in young oceanic crust where basement outcrops penetrate the sediment and allow seawater inflow and outflow (e.g., Lister, 1972; Fisher et al., 1990; Hutnak et al., 2008; Anderson et al., 2012). The eastward increase in heat flow across the sediment pond, from younger to older crust, is consistent with fluid flow from west to east. Given the bathymetry of the fracture zone bounding the sediment pond (Figs. 2, 3 and 4), recharge could occur through exposed basement relief along the western margin of the sediment pond. The discharge in the east likely occurs at the poorly sedimented basement exposure where a possible normal fault intersects the seafloor (Fig. 4). The distance between the interpreted recharge and discharge areas is ~ 9300 m. The small outcrop on the west is chosen as the recharge zone, but the recharge region could be somewhat broader. Note there is another, smaller sediment pond to the east (Fig. 3) for which we have no heat flow data. Given its topography and sediment cover, there could also be advective heat transfer within it.

To determine the redistribution of heat by lateral flow through the basement, we apply the well-mixed aquifer model first derived by Langseth and Herman (1981) and subsequently used by
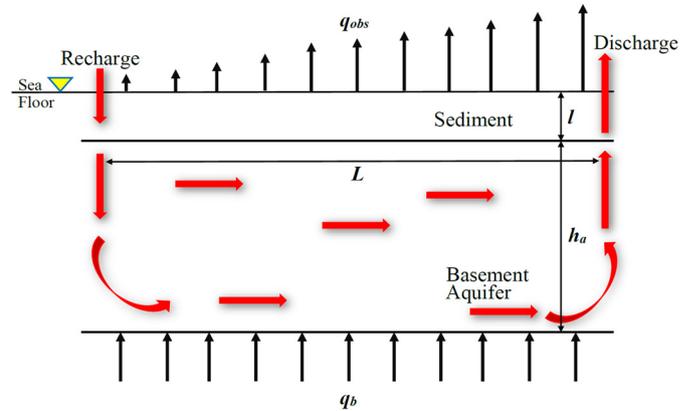
Fig. 5. A well-mixed aquifer flow model modified from Langseth and Herman (1981), Fisher and Becker (2000). Refer to Table 2 for parameters shown in this figure.

Fisher and Becker (2000), Rosenberg et al. (2000) and Anderson et al. (2012) to describe outcrop-to-outcrop hydrothermal circulation. In this model, water absorbs the heat transferred from the lithosphere below and as it flows laterally in the highly-porous, igneous basement it simultaneously loses heat by conduction to the overlying sediment layer (Fig. 5). Assuming advection of heat is much greater than lateral conduction in the aquifer, the steady state thermal balance can be expressed as (Langseth and Herman, 1981),

$$\rho_f c_f u h_a \frac{dT(x)}{dx} = q_b - K_s \frac{T(x)}{l}. \qquad (5)$$

Solving equation (5) with boundary condition, $T = T_0$ at $x = x_0$, yields,

$$\frac{q(x)}{q_b} = 1 + \left(\frac{q(x_0)}{q_b} - 1 \right) \left[e^{\frac{a^*}{u h_a l}(x_0 - x)} \right], \qquad (6)$$

where $a^* = K_s / \rho_f c_f$; $q(x)$ is heat flow at distance of x from x_0; $q(x_0)$ is the heat flow at distance x_0; x_0 is the distance of the first
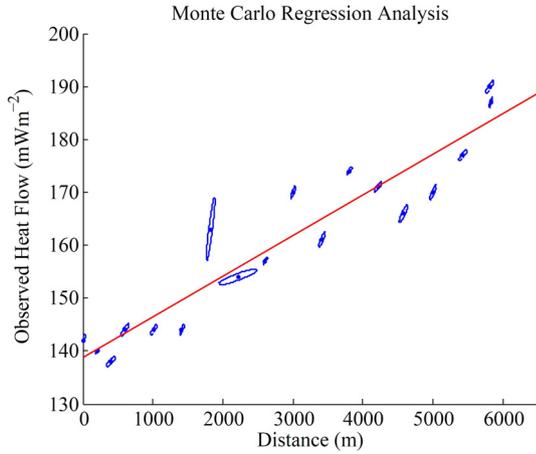
Fig. 6. Regression analysis of the conductive heat flow measurements based on Monte Carlo simulation. 18 heat flow determinations and their measurement and distance uncertainties as a function of distance. Slope $= 0.008 \pm 0.001$ mW m^{-3} and Intercept $= 139 \pm 5$ mW m^{-2} are used in equation (7) to determine the volumetric flow rate through the basement aquifer.

heat flow measurement from the recharge outcrop (see in Table 1). To determine the volumetric flow rate, uh_a, per unit length perpendicular to the heat flow profile, we note that the heat flow data follow a nearly linear trend from west to east along the profile. We therefore assume the exponential term in equation (6) is small and expand the exponential in a Taylor expansion leading to a linear expression for $q(x)$,

$$q(x) = q(x_0) + \frac{a^*}{uh_a l}\big(q(x_0) - q_b\big)(x_0 - x). \tag{7}$$

By performing a Monte Carlo simulation (using MATLAB) for regression analysis, we obtain an estimate of 0.008 ± 0.001 mW m^{-3} for the slope $(a^*/uh_a l)(q(x_0) - q_b)$ that fits the data (Fig. 6) to within the 95% confidence interval and yields an estimate for the volumetric flow rate per unit length, uh_a, of $\sim 400 \pm 250$ m^2 yr^{-1}.

We estimate the permeability, k, of the crustal aquifer by using the flow rate uh_a derived from equation (7) in Darcy's Law:

$$uh_a = -\frac{kh_a}{\eta}\nabla P, \tag{8}$$

where η is the dynamic viscosity of the fluid and ∇P is the pressure gradient driving the flow. We write Darcy's Law in this form because the aquifer thickness is unknown and only the product uh_a can be estimated directly from the heat flow data. Following Fisher and Becker (2000), we assume that the pressure gradient driving the flow uh_a results from the buoyancy difference between the cold seawater entering the aquifer and the warmer fluid exiting it. Neglecting flow resistance in the recharge and discharge outcrops, equation (8) can be written as,

$$uh_a = \frac{\alpha g k \Delta T h_a (h_a + l)}{\nu L}, \tag{9}$$

where α is thermal expansion coefficient of water; g is the acceleration due to gravity; ΔT is the temperature difference between recharge and discharge; L is length of the horizontal fluid flow path, and ν is the kinematic viscosity of the fluid. Because the aquifer thickness occurs independently in equation (9) through the term $h_a + l$, to determine k, one needs to estimate both h_a and ΔT in equation (9). To obtain a reasonable range of estimates for k, we consider $h_a = 100$ m and 1000 m. By assuming that fluid enters the aquifer at the seawater temperature, taken to be 0 °C, and exits at the temperature of the sediment-basement interface at the end of the flow path L, we obtain an upper estimate of ΔT. Extrapolating the linear fit for the observed heat flow data, from equation

(7), to 9300 m as shown in Fig. 4(b), we estimate heat flow at the discharge, $q_d \approx 210$ mW m^{-2}. Writing the one-dimensional conductive heat flow equation as,

$$q_d = K_s \frac{T_d}{l}, \tag{10}$$

yields $T_d \approx 80$ °C, which is then the value of ΔT. Substituting this value of ΔT in equation (9), along with a mean sediment thickness $l = 260$ m, other parameters from Table 2, and $uh_a = 400$ m^2 yr^{-1}, we obtain permeabilities of $\sim 10^{-11}$ and 10^{-12} m^2 for aquifer thicknesses of 100 and 1000 m, respectively.

5. Discussion

5.1. Robustness of the model

The mean conductive heat flow obtained across a sediment basin in the inactive part of the EFZ reported in this paper ranges between $\approx 40\%$ and $\approx 80\%$ of the predicted heat flow. The heat flow increases nearly linearly from west to east, which is opposite to that expected based on the age of the oceanic crust on either side of the fracture zone. A seismic reflection profile along the heat flow profile shows that sediment thickness varies irregularly but tends to increase from west to east and that the basin is bounded by outcrops, potentially allowing for seawater to enter and exit the crust. To interpret the observed heat flow deficit and the west to east increase in heat flow through the sediment, we constructed a 1D well-mixed aquifer model, which indicates that homogeneous west to east lateral flow through the basement rocks at an average flow rate of $\approx 400 \pm 250$ m^2 yr^{-1} per unit length perpendicular to the heat flow profile can explain the data. Assuming flow is driven by convection resulting from a temperature difference of ~ 80 °C between the recharge and discharge sites, the aquifer permeability is estimated to range from $\sim 10^{-11}$ m^2 to 10^{-12} m^2 for aquifer thickness between 100 m and 1000 m, respectively.

Key assumptions in the analysis presented in the previous section are that: (1) the well-mixed aquifer model is appropriate and (2) the temperature difference driving the flow is maximum, corresponding to the difference between cold seawater and the basement temperature near the discharge site.

The well-mixed aquifer model assumes that the temperature and flow rate do not vary significantly with depth in the basement. To explore this assumption, we consider the possibility that fluid convection is occurring in the basement rocks. For a porous layer with a given heat flux at the base and a fixed temperature at the surface, thermal convection occurs when the Rayleigh number, Ra, exceeds a critical value, Ra_c. Assuming the sediment and the base of the basement aquifer are impermeable, Nield (1968) shows that

$$Ra = \frac{\alpha g k \Delta T h_a}{a_b^* \nu} \geq Ra_c = 27.1, \tag{11}$$

where $\Delta T = q_b h_a / K_b \approx 15$ °C and ≈ 150 °C for $h_a = 100$ m and 1000 m, respectively, is the temperature difference across the conducting layer, effective thermal diffusivity of basement rocks, $a_{b*} = K_b / \rho_f c_f \approx 5 \times 10^{-7}$ m^2 s^{-1} and K_b is the thermal conductivity of the basement rocks. From equation (11), the derived permeabilities of the aquifer, for $Ra_c = 27.1$, for $\Delta T = \approx 15$ °C and 150 °C are $\sim 10^{-11}$ m^2 and 10^{-13} m^2, respectively. For a vigorous convection to occur in the aquifer, we assume $Ra = 100 \times Ra_c$. Based on this Ra, for $\Delta T \approx 15$ °C and ≈ 150 °C permeabilitites of $\sim 10^{-9}$ m^2 and $\sim 10^{-11}$ m^2 are obtained. The permeability values for vigorous convection in the aquifer are somewhat higher than the values obtained from equation (9), but are not unrealistic. Moreover, the k values determined from equation (9) indicate that the aquifer beneath the sediment pond is likely to be convecting, which would

tend to homogenize the temperature distribution in the aquifer, except at boundary layers. Therefore the application of the well-mixed aquifer model is reasonable.

Another way to estimate the temperature difference driving the flow through the aquifer is to recognize that the mean heat flow deficit is ≈140 mW m^{-2}. Integrated along the west to east length of the basin, this corresponds to a total advective heat loss $H \approx 1.3 \times 10^6$ mW m^{-1}. Using the mean volumetric flow rate per unit length determined from equation (7), we can obtain a new estimate of ΔT. Writing,

$$H = \rho_f c_f u h_a \Delta T, \tag{12}$$

Equation (12) gives $\approx30\,°C$. This estimate is considerably less than $\Delta T \approx 80\,°C$ used in equation (9) to determine the permeability. This smaller value of ΔT suggests that thermal conduction may have warmed the recharge fluid or cooled the discharge fluid. Using $\Delta T = 30\,°C$ in equation (9) yields an estimate of $k \sim 10^{-10}$ m^2 and 10^{-12} m^2 for $h_a = 100$ m and 1000 m respectively. These higher values of permeability further support the validity of the aquifer model. We also recognize that a maximum value of ΔT was used in calculating k in the analysis section when compared to the one used above. As can be seen in Fig. 3, the length of the horizontal flow path, L, is a minimum. If recharge occurred through a larger part of the elevated topographic feature at the western boundary of the sediment pond, L would be somewhat longer than estimated, the buoyancy difference driving the flow would be smaller, and the corresponding permeability would be slightly larger. The uncertainty in the aquifer thickness, h_a, is much greater than the uncertainty in L, however, so small changes in L would not change the estimated basement permeability appreciably.

The estimates of crustal permeability derived in this paper for the Ecuador Fracture Zone are similar to estimates in ridge flank environments in other settings (Fisher, 1998), and similar to those obtained at Hole 504b (Becker et al., 1983; Carlson, 2011). Given our limited knowledge of the basement structure and its permeability, however, we cannot conclude whether a 100 m or a 1000 m thick aquifer is more appropriate for this region.

5.2. Implications of the results

In the analysis presented here, the $\approx50\%$ heat deficit in the observed heat flow implies that the mean advective heat flow $q_{adv} = 140$ mW m^{-2}. For a ~10 km long aquifer length and assuming a ~10 km length perpendicular to the heat flow profile, the total advective heat output from a 10 km^2 area is ≈0.15 MW. This heat output is small compared to the heat output of the ridge-crest hydrothermal systems, which is ~100 MW over a smaller area of 10^3–10^4 m^2. Hence on a global scale it would not appear that hydrothermal heat loss from fracture zones is significant.

Roland et al. (2010) develop a numerical model of the thermal regime of the active transform region between two ridge segments. In their model, they parameterize the effect of hydrothermal circulation by an enhanced thermal conductivity that is a function of a depth-dependent Nusselt number. Their model does not consider the inactive fracture zone extension. Currently, the only model for heat transfer in the fracture zone extension involves lateral conductive heat transfer from the younger to the older plate (Louden and Forsyth, 1976). This model has then been used to explain the geoid and topographic signatures of fracture zone extensions as they age (e.g., Sandwell and Schubert, 1982; Sandwell, 1984; Pockalny et al., 1996). The heat flow profile reported here for the Ecuador Fracture Zone shows that lateral heat advection via outcrop-to-outcrop fluid flow may significantly increase the rate of heat transfer from the younger to the older plate and hence might

affect the topographical evolution and geoid signatures of fracture zones. Additional heat flow studies are needed to confirm such effects.

6. Conclusions

Based on our analysis of a set of 18 conductive heat flow measurements in a sediment pond in the EFZ, we conclude the following:

1. The mean conductive heat flow is ~160 mW m^{-2} which is $\approx50\%$ of the mean basal heat flux yielded by a pure conduction model.
2. For rapid sedimentation to depress heat flow, the sediments should have been emplaced a relatively short time ago of $\sim10,000$ yr to explain the heat flow deficit.
3. Lateral advective heat transfer by fluids flowing from a recharge outcrop in the west to the discharge fault in the east is consistent with the eastward increase in heat flow values and could explain the deficit in heat flow.
4. Applying a well-mixed aquifer model to determine the redistribution of heat flow through the basement, we estimate a mean volumetric flow rate of ≈400 m^2 yr^{-1}.
5. Estimates of permeabilities in the basement, based on the mean volumetric flow rate, are $\sim10^{-11}$ and 10^{-12} m^2 for aquifer thicknesses of 100 and 1000 m, respectively.
6. Based on the Rayleigh number analysis for onset of fluid convection and vigorous convection in the basement rocks, the permeability estimates further support the application of the well-mixed aquifer model.

Therefore, the heat flow data in the EFZ shows that lateral heat advection is likely an important heat transfer mechanism in fracture zones. The analysis of the rate of heat transfer using a simple well mixed aquifer model suggests that crustal permeability of the fracture zones is similar to that of typical oceanic crust. Lateral advective heat transfer from the young to old plate significantly enhances the rate of lateral heat transfer obtained from conduction models. Outcrop-to-outcrop lateral heat transfer in fracture zones may affect the evolution of fracture zones as they age, but additional studies are needed to confirm the general importance of this process.

Given the lack of heat flow studies in transform and fracture zone settings, our model and results could be used to constrain models of fracture zone settings and also transform faults. Our study demonstrates that our understanding of these pervasive geological features is incomplete. To address this issue, the acquisition of more heat flow data along with other geological and geophysical data would make a significant contribution to our understanding of the role of fluid flow and advective heat transport in oceanic fracture zones.

Acknowledgements

References

Anderson, B.W., Coogan, L.A., Gillis, K.M., 2012. The role of outcrop-to-outcrop fluid flow in off-axis oceanic hydrothermal systems under abyssal sedimentation conditions. J. Geophys. Res. 117, B05103. http://dx.doi.org/10.1029/2011JB009052.

Becker, K., Langseth, M.G., Von Herzen, R.P., Anderson, R.N., 1983. Deep crustal geothermal measurements, hole 504B, Costa Rica Rift. J. Geophys. Res., Solid Earth 88 (B4), 3447–3457.

Behn, M.D., Boettcher, M.S., Hirth, G., 2007. Thermal structure of oceanic transform faults. Geology 35 (4), 307–310.

Carlson, R.L., 2011. The effect of hydrothermal alteration on the seismic structure of the upper oceanic crust: evidence from Holes 504B and 1256D. Geochem. Geophys. Geosyst. 12 (9).

Dziak, R.P., Fox, C.G., Embley, R.W., Nabelek, J.L., Braunmiller, J., Koski, R.A., 2000. Recent tectonics of the Blanco Ridge, eastern Blanco transform fault zone. Mar. Geophys. Res. 21 (5), 423–450.

Fisher, A.T., 1998. Permeability within basaltic oceanic crust. Rev. Geophys. 36, 143–182.

Fisher, A.T., Becker, K., Narisimhan, T.N., Langseth, M.G., Mottl, M.J., 1990. Passive, off-axis convection near the southern flank of the Costa Rica Rift. J. Geophys. Res. 95, 9343–9370.

Fisher, A.T., Becker, K., 2000. Channelized fluid flow in oceanic crust reconciles heat-flow and permeability data. Nature 403, 71–74.

Hey, R., Johnson, G.L., Lowrie, A., 1977. Recent plate motions in the Galapagos area. Geol. Soc. Am. Bull. 88 (10), 1385–1403.

Hutchison, I., 1985. The effects of sedimentation and compaction on oceanic heat flow. Geophys. J. Int. 82 (3), 439–459.

Hutnak, M., Fisher, A.T., 2007. Influence of sedimentation, local and regional hydrothermal circulation, and thermal rebound on measurements of seafloor heat flux. J. Geophys. Res., Solid Earth 112 (B12).

Hutnak, M., Fisher, A.T., Harris, R., Stein, C., Wang, K., Spinelli, G., Schindler, M., Villinger, H., Silver, E., 2008. Large heat and fluid fluxes driven through mid-plate outcrops on ocean crust. Nat. Geosci. 1, 611–614.

Kastens, K.A., Macdonald, K.C., Miller, S.P., Fox, P.J., 1986. Deep tow studies of the Vema Fracture Zone: 2. Evidence for tectonism and bottom currents in the sediments of the transform valley floor. J. Geophys. Res., Solid Earth 91 (B3), 3355–3367.

Langseth, M.G., Le Pichon, X., Ewing, M., 1966. Crustal structure of the mid-ocean ridges: 5. Heat flow through the Atlantic Ocean floor and convection currents. J. Geophys. Res. 71 (22), 5321–5355.

Langseth, M.G., Hobart, M.A., 1976. Interpretation of heat flow measurements in the Vema fracture zone. Geophys. Res. Lett. 3 (5), 241–244.

Langseth, M.G., Herman, B.M., 1981. Heat transfer in the oceanic crust of the Brazil Basin. J. Geophys. Res. 86, 10805–10819.

Lister, C.R.B., 1972. On the thermal balance of a mid-ocean ridge. Geophys. J. Int. 26 (5), 515–535.

Louden, K.E., Forsyth, D.W., 1976. Thermal conduction across fracture zones and the gravitational edge effect. J. Geophys. Res. 81 (26), 4869–4874.

Menard, H.W., Atwater, T., 1969. Origin of fracture zone topography. Nature 222, 1037–1040.

Nield, D.A., 1968. The Rayleigh–Jeffreys problem with boundary slab of finite conductivity. J. Fluid Mech. 32 (02), 393–398.

Pockalny, R.A., Gente, P., Buck, R., 1996. Oceanic transverse ridges: a flexural response to fracture-zone–normal extension. Geology 24 (1), 71–74.

Roland, E., Behn, M.D., Hirth, G., 2010. Thermal-mechanical behavior of oceanic transform faults: implications for the spatial distribution of seismicity. Geochem. Geophys. Geosyst. 11 (7).

Rosenberg, N.D., Fisher, A.T., Stein, J.S., 2000. Large-scale lateral heat and fluid transport in the seafloor: revisiting the well-mixed aquifer model. Earth Planet. Sci. Lett. 182 (1), 93–101.

Sandwell, D.T., Schubert, G., 1982. Geoid height-age relation from SEASAT altimeter profiles across the Mendocino Fracture Zone. J. Geophys. Res., Solid Earth 87 (B5), 3949–3958.

Sandwell, D.T., 1984. Thermomechanical evolution of oceanic fracture zones. J. Geophys. Res. 89 (B13), 11401–11413.

Stein, C.A., Stein, S., 1994. Constraints on hydrothermal heat flux through the oceanic lithosphere from global heat flow. J. Geophys. Res. 99, 3081–3095.

Stein, J.S., Fisher, A.T., 2001. Multiple scales of hydrothermal circulation in Middle Valley, northern Juan de Fuca Ridge: physical constraints and geologic models. J. Geophys. Res., Solid Earth 106 (B5), 8563–8580.

Tuckwell, G.W., Bull, J.M., Sanderson, D.J., 1996. Models of fracture orientation at oblique spreading centres. J. Geol. Soc. 153 (2), 185–189.

Vacquier, V., Von Herzen, R.P., 1964. Evidence for connection between heat flow and the mid-Atlantic ridge magnetic anomaly. J. Geophys. Res. 69 (6), 1093–1101.

Villinger, H., Davis, E.E., 1987. A new reduction algorithm for marine heat flow measurements. J. Geophys. Res., Solid Earth 92 (B12), 12846–12856.

Von Herzen, R., Simmons, G., 1972. Two heat flow profiles across the Atlantic Ocean. Earth Planet. Sci. Lett. 15 (1), 19–27.